Observing continuous-variable geometric phase and implementing geometric entangling gates in a superconducting circuit

Chao Song,[1] Shi-Biao Zheng,[2, a)] Pengfei Zhang,[1] Kai Xu,[1] Libo Zhang,[1] Qiujiang Guo,[1] Wuxin Liu,[1] Da Xu,[1] Hui Deng,[3] Keqiang Huang,[3] Dongning Zheng,[3] Xiaobo Zhu,[3, 4, b)] and H. Wang[1, 4, c)]

[1)] *Department of Physics, Zhejiang University, Hangzhou, Zhejiang 310027, China*
[2)] *Department of Physics, Fuzhou University, Fuzhou, Fujian 350116, China*
[3)] *Institute of Physics, Chinese Academy of Sciences, Beijing 100190, China*
[4)] *Synergetic Innovation Center of Quantum Information and Quantum Physics, University of Science and Technology of China, Hefei, Anhui 230026, China*

(Dated: 30 November 2016)

Geometric phase, associated with holonomy transformation in quantum state space, is an important quantum-mechanical effect[1–3], which has close relations with a variety of physical phenomena in areas including optics, molecular physics, quantum field theories, and condensed matter physics[4,5]. In addition to fundamental interest, this geometric effect has many important practical applications, among which the geometric quantum computation is a paradigm, where quantum logic operations are realized through geometric phase manipulations with intrinsic noise-resilient advantages[6,7]. So far, this effect has been detected in a number of discrete-variable systems with finite-dimensional Hilbert space[7–16]; however, experimental observation of a phase entirely produced by holonomy transformation for continuous variables is still lacking. Here we report on the first experimental observation of such a purely geometric phase for a continuous-variable bosonic mode realized with a microwave resonator, whose quantum state is parallel-transported along a closed loop in the projected Hilbert space conditional on the state of a superconducting qubit. The observed phase is due to the holonomy effect associated with this transport. Based on this phase, we demonstrate the first realization of the geometric two-qubit controlled-phase and three-qubit controlled-controlled-phase gates in a superconducting circuit. Our results represent a significant advance in the experimental exploration of continuous-variable geometric phase, and a key step towards implementation of geometric quantum computation in superconducting integrated circuits.

A quantum system, when undergoing a cyclic evolution in the quantum state space, will acquire a geometric phase that is proportional to the area enclosed by the circuit[1,2]. This effect was first discovered by Berry, who showed that a quantum system, initially in a nondegenerate eigenstate of an adiabatically and cyclically varied Hamiltonian, will eventually return to the initial state, but pick up a phase factor of geometric origin[1]. Unlike the time- and energy-dependent dynamical phase, geometric phase is due to holonomy transformation associated with the parallel transport of the quantum state, whose magnitude is only determined by the area enclosed by the cyclic trajectory in the projected Hilbert space[2]. As such, geometric phase is robust against certain types of noise perturbations that deform the path but preserve the enclosed area, which makes itself a favorable choice for noise-resilient coherent manipulation of quantum states and for high-fidelity quantum computation[6,7]. The behaviors of geometric phases subject to different noise sources have been investigated for both the adiabatic and nonadiabatic evolutions. The effects of random fluctuations of classical control parameters on Berry's phase of a spin-1/2 in a slowly changing magnetic field have been analyzed theoretically, showing the robustness of geometric phase against classical noises[22]. In addition, it has been shown that geometric phase is insensitive to decoherence effects arising from coupling to reservoirs[23,24].

So far, Berry's phase and its extensions in various discrete-variable systems, e.g., qubits, have been experimentally investigated[8–12] and used for realization of elementary quantum gates[7,13–16]. However, phases of purely geometric origin have not been observed in continuous-variable systems, or harmonic oscillators whose states are defined in an infinite-dimensional Hilbert space. Although the geometric phase of a harmonic vibrational mode of trapped ions has been utilized for implementing high-fidelity quantum gates[6], the evolution does not satisfy the parallel-transport condition, and thus the total phase acquired by the system involves a dynamical component that is opposite in sign and twice the size of the nonadiabatic, or Aharonov-Anandan, geometric phase[2], as shown in Ref.[25]. In a recent experiment[26], the adiabatic geometric phase of the quantized electromagnetic field stored in a resonator was measured in a superconducting circuit quantum electrodynamics (QED) system. However, the observed total phase contains a dynamical contribution that is much larger than the geometric phase itself, which makes the procedure sensitive to parameter

[a)] Electronic mail: t96034@fzu.edu.cn
[b)] Electronic mail: xbzhu16@ustc.edu.cn
[c)] Electronic mail: hhwang@zju.edu.cn

fluctuations and hence unfavorable for implementation of noise-resilient geometric quantum computation. Superconducting integrated circuits provide a scalable solid-state platform for quantum information processing, but where the geometric approach has been experimentally limited to the realization of single-qubit gates[13].

Here we propose and realize a scheme for observation of the geometric phase of an electromagnetic resonator with a superconducting circuit QED system, and for implementation of entangling gates with up to three qubits based on this phase. The device features up to five Xmon qubits, labeled from Q_1 to Q_5, coupled to a central bus resonator, R (see Fig. 1a, Methods, and Supplementary Information). In our experiment, the state of the resonator is parallel-transported along a circuit in the projected Hilbert space conditional on the state of the qubit coupled to the resonator, so that the total phase measured by the Ramsey interference experiment is of purely geometric origin. Using this phase, we realize the two-qubit controlled-phase (CZ) gate and the three-qubit controlled-controlled-phase (CCZ) gate—the equivalent of the Toffoli gate under a change of the target basis. The geometric CZ gate is calibrated by quantum process tomography (QPT) and randomized benchmarking (RB), each giving a fidelity of about 0.94; the CCZ gate, achieved without resorting to the two-qubit-gate decomposition, has a QPT fidelity of 0.868 ± 0.004, which compares favorably to the results obtained by step-by-step dynamical approaches[17–21].

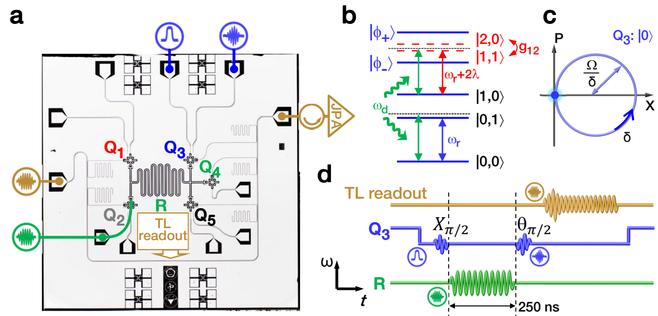

FIG. 1. **Device and scheme for measuring the geometric phase.** **a**, Device image illustrating the five frequency-tunable qubits and the central bus resonator R which has a fixed bare frequency (resonator frequency in absence of qubits) $\omega_{rb}/2\pi \approx 5.585$ GHz. The color-coded icons identify the pads where pulses are injected onto the circuit chip. The transmission line (TL) line carries the multi-tone microwave pulse through the circuit chip, which is amplified by a Josephson parametric amplifier (JPA) at low temperature and then demodulated at room temperature to yield the state of all qubits. **b**, Energy level configuration of the qubit-resonator system. The strong coupling between $|2,0\rangle$ and $|1,1\rangle$ produces the dressed states $|\phi_\pm\rangle$ whose energy levels are well separated. A microwave drive with a tone of ω_d that is slightly detuned from ω_r by δ can or cannot excite the resonator depending on whether the qubit is in the state $|0\rangle$ or $|1\rangle$. **c**, Resonator's phase-space displacement conditional on the qubit state $|0\rangle$. The resonator, initially in its ground state, is displaced by the microwave drive of an amplitude Ω, along a circle in phase space with the radium Ω/δ and the angular velocity δ conditional on the qubit state $|0\rangle$. At time $T = 2\pi/\delta$ the resonator makes a cyclic evolution, returning to the ground state, but acquires a conditional geometric phase proportional to the enclosed phase-space area. **d**, Ramsey interference sequence plotted in the frequency versus time plane. The geometric operation, resulting from the combination of the microwave drive (green sinusoid) and the qubit-resonator coupling, is sandwiched in between the two $\pi/2$ rotations (blue sinusoids with Gaussian envelopes), $X_{\pi/2}$ and $\theta_{\pi/2}$, whose rotation axes are in the xy plane of the Bloch sphere and differ by an angle of θ. The corresponding geometric phase β is revealed by measuring the qubit $|1\rangle$-state probability as a function of θ, using the microwave pulse through the TL readout line (light brown sinusoid with a ring-down shape at the beginning).

First we introduce the single-qubit experiment for observing the resonator's pure geometric phase, measured through Q_3's Ramsey interference. The qubit-resonator level configuration is illustrated in Fig. 1b, where c and d in the joint state $|c,d\rangle$ denote the excitation numbers of the qubit and the resonator, respectively. The qubit $|0\rangle \leftrightarrow |1\rangle$ transition at the tone ω_{01} is coupled to the resonator with a coupling strength $g_{01}/2\pi = 20.1$ MHz. When the qubit-resonator detuning Δ ($\equiv \omega_{01} - \omega_{rb}$) is much larger than g_{01} so that the energy levels $|1,0\rangle$ and $|0,1\rangle$ are well separated as illustrated in Fig. 1b, there is no population exchange between these two levels; the dispersive coupling results in a qubit-state-dependent resonator frequency shift, described by the effective Hamiltonian $\hbar\lambda\left(|1\rangle\langle 1| - |0\rangle\langle 0|\right)a^\dagger a$, where $a^\dagger$ and a are the creation and annihilation operators for the photons stored in the resonator, $\hbar$ is the Planck constant, and $\lambda = g_{01}^2/\Delta$. The resonator is off-resonantly driven by an external microwave field with the amplitude Ω and the frequency ω_d. When the qubit is initially in the state $|0\rangle$, it remains in this state, and the effective Hamiltonian for the driven resonator, in the frame rotating at ω_d, becomes

$$H = -\hbar\delta a^\dagger a + \hbar\Omega(a + a^\dagger), \tag{1}$$

where $\delta = \omega_d - \omega_r$ and ω_r ($\equiv \omega_{rb} - \lambda$) denotes the resonator frequency conditional on the qubit state $|0\rangle$. After a time t, the resonator evolves from the ground state to the coherent state $|\phi(t)\rangle = e^{i\beta(t)}|\alpha(t)\rangle$, where $\beta(t) = -\frac{\Omega^2}{\delta}[t - \frac{1}{\delta}\sin(\delta t)]$, and $\alpha(t) = \frac{\Omega}{\delta}(1 - e^{i\delta t})$ is the complex amplitude of the coherent field. After a time $T = 2\pi/\delta$, the resonator makes a cyclic evolution, returning to the initial state but acquiring a phase, $\beta = -2\pi(\Omega/\delta)^2$. One important feature of this evolution is that it satisfies the parallel-transport condition $\langle\phi(t)|\,\frac{d}{dt}\,|\phi(t)\rangle = 0$. As a consequence, no dynamical phase is accumulated during the evolution. Although arising from the holonomy transformation associated with the parallel transport in the projected Hilbert space, the geometric phase β is best visualized in phase space spanned by the two quadratures $X = (a + a^\dagger)/2$ and $P = (a - a^\dagger)/2i$, where the resonator state moves around a circle with the radium Ω/δ and angular velocity δ, as shown in Fig. 1c; β is proportional to the enclosed phase-space area. We note that the parallel-transport condition was not satisfied in ion-trap experiments[6], and thus the phase used for entangling the ion-qubits is not a holonomy in the projected

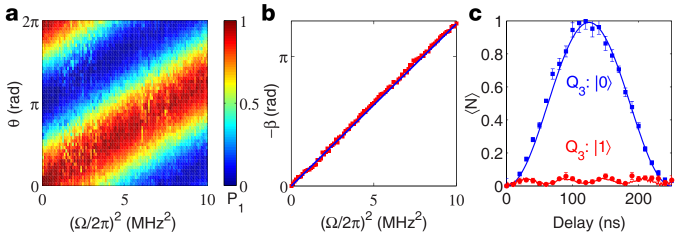

FIG. 2. **Ramsey interference signal and resonator photon number evolution.** **a,** Occupation probability P_1 of Q_3 in $|1\rangle$ as a function of θ and Ω^2, which is measured using the pulse sequence shown in Fig. 1d with the drive detuning $\delta/2\pi = 4$ MHz. **b,** $-\beta$ versus Ω^2 (red dots), where β is obtained by tracing the P_1-maximum contour in **a**: For each Ramsey trace of P_1 versus θ sliced along a fixed Ω^2, we perform the cosinusoidal fit with the phase offset giving the value of β. The blue solid line shows the theoretical result. **c,** Measured average photon numbers with error bars of the resonator as functions of time during the application of the microwave drive with $\Omega/2\pi = 2$ MHz conditional on the qubit states $|0\rangle$ (blue dots) and $|1\rangle$ (red dots). Lines are the numerical results.

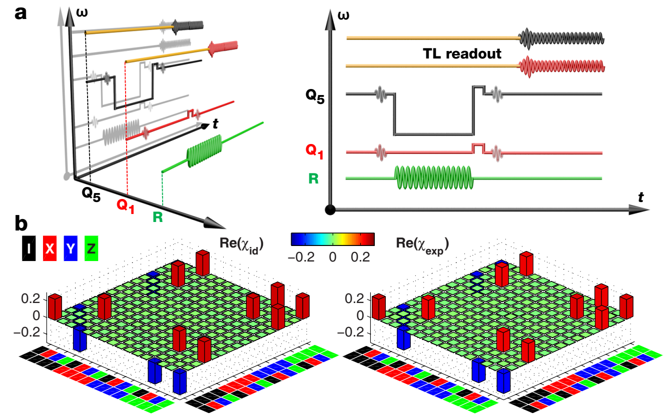

FIG. 3. **QPT of the geometric two-qubit CZ gate,** obtained with the drive amplitude $\Omega/2\pi = \sqrt{7.0}$ MHz and detuning $\delta/2\pi = 4$ MHz. **a,** Pulse sequences illustrated in three dimensions (left) and projected to two dimensions (right), with the axes as labeled. For each qubit, the first sinusoid with a Gaussian envelope is for state preparation, which is varied to generate one of the four states $\{|0\rangle, (|0\rangle - i|1\rangle)/\sqrt{2}, (|0\rangle + |1\rangle)/\sqrt{2}, |1\rangle\}$; the second sinusoid with a Gaussian envelope is also variable, acting as the rotation pulse needed in QST; sandwiched in between the two sinusoids is the big square pulse used to adjust the qubit energy levels of Q_5 (there is no frequency adjustment on Q_1), which combines with the resonator microwave drive to fulfill the CZ gate; the next small square pulse produces a single-qubit rotation on each qubit to partially compensate for the dynamical phase accumulated during the CZ gate; finally qubits are measured by demodulation of the two-tone microwave through the TL readout line (light brown lines with color-coded sinusoids). Here the readout and gate frequencies of Q_5 are different for minimizing the Q_1-Q_5 interaction during readout. **b,** Ideal ($\chi_{\rm id}$, left) and experimental ($\chi_{\rm exp}$, right) quantum process matrices. The color code for Pauli basis {I, X, Y, Z} is shown at the top-left corner. Imaginary components of $\chi_{\rm exp}$ are measured to be no larger than 0.015 in magnitude. $\chi_{\rm exp}$ has a fidelity $F = \mathrm{Tr}\,(\chi_{\rm id}\chi_{\rm exp}) = 0.936 \pm 0.013$. The $|2\rangle$-state occupation probability of each qubit averaged over the 16 output states is no higher than 0.015 in a separate measurement.

Hilbert space, though both the dynamical and geometric components are proportional to the enclosed phase-space area[25].

The strong coupling between the qubit-resonator states $|1,1\rangle$ and $|2,0\rangle$ is used to freeze the resonator's evolution associated with the qubit state $|1\rangle$. When these two states are on near resonance, they are strongly coupled and form two dressed states $|\phi_\pm\rangle$ with modified energy levels that are separated by about g_{12} (see Supplementary Information), where g_{12} ($\approx \sqrt{2}g_{01}$) is the coupling strength between the qubit $|1\rangle \leftrightarrow |2\rangle$ transition and the resonator (Fig. 1b). Under the weak driving condition $\Omega \ll g_{12}$, the external field cannot drive the system to evolve from the state $|1,0\rangle$ to either one of $|\phi_\pm\rangle$, but shifts its energy level and produces a dynamical phase. We eliminate this dynamical phase by adjusting the qubit-resonator detuning so that the energy shifts associated with the off-resonant couplings to $|\phi_\pm\rangle$ cancel each other. Under this condition, nothing changes when the qubit is in $|1\rangle$ (see detailed calculations in Supplementary Information). The geometric phase acquired by the resonator can be encoded in the relative probability amplitude of the qubit basis states $|0\rangle$ and $|1\rangle$ and measured in a Ramsey interference experiment.

During the application of the resonator drive, the $|0\rangle \leftrightarrow |1\rangle$ and $|1\rangle \leftrightarrow |2\rangle$ transitions of Q_3 are blue-detuned from the resonator $\omega_r/2\pi$ by 284 MHz and 39 MHz, respectively. The resulting geometric phase is observed by the Ramsey-type measurement, where the above-mentioned geometric operation is sandwiched in between two $\pi/2$ rotations on Q_3 as illustrated in Fig. 1d (also see Methods). In Fig. 2a we present the measured probability of Q_3 in $|1\rangle$ after the second $\pi/2$ rotation, P_1, as a function of θ and Ω^2 in a two-dimensional colormap, where Ω is calibrated by measuring the drive-generated resonator photon number with Q_4. Tracing the contour of the P_1 maximum yields the linear dependence of the negative geometric phase, $-\beta$, on Ω^2, which agrees exceptionally well with the analytic solution (solid line) and thus indicates that the observed phase is of purely geometric origin (Fig. 2b). Figure 2c displays the average photon numbers with error bars of the resonator as functions of time during application of the drive with Q_3 in $|0\rangle$ (blue) and $|1\rangle$ (red), which are measured by tuning Q_4, initially in its ground state, on resonance with the resonator for an interaction time before its readout; the resulting P_1 versus time curve is used to extract the photon populations. As expected, when Q_3 is in the state $|1\rangle$, the resonator almost remains unpopulated; for the qubit state $|0\rangle$, the resonator makes a cyclic evolution, returning to the ground state after the duration $T = 250$ ns.

Now we turn to the implementation of a geometric CZ gate with Q_1 and Q_5: The $|1\rangle \leftrightarrow |2\rangle$ transitions of both qubits are tuned on near resonance with the resonator, and therefore the $|0\rangle \leftrightarrow |1\rangle$ transitions of both qubits are dispersively coupled to the resonator due to the large qubit anharmonicities; the detuning between Q_1 and Q_5 is kept much larger than the dispersive coupling strengths to minimize the resonator-induced qubit excitation exchange. With these settings, the external microwave field will drive the resonator to traverse a circle in phase space when both qubits are in the state $|0\rangle$; when one qubit is in $|1\rangle$, the strong coupling between the joint states $|1,1\rangle$ and $|2,0\rangle$ of this qubit and the resonator is again used to freeze the resonator's evolution for the same reason outlined in the single-qubit experiment, and so is the case when both qubits are in $|1\rangle$ (see Supplementary Information). A geometric two-qubit phase gate can thus be constructed, where a geometric phase β is produced if and only if both qubits are in the state $|0\rangle$.

To examine the phase acquired by each of the two-qubit computational states during the gate operation, we perform the Ramsey-type measurements on each qubit with the other qubit in $|0\rangle$ and $|1\rangle$, respectively (see Supplementary Information). In addition to the dominant Ω^2-dependent geometric phase β gained by $|00\rangle$, the Ramsey data show that the two-qubit computational states also accumulate different but small dynamical phases, which constitute the majority of phase errors to the CZ gate in our experimental realization. We perform additional single-qubit rotations to partially compensate for the dynamical-phase-induced errors.

To characterize the resulting CZ gate, the two-qubit QPT is performed by creating 16 distinct two-qubit input states and mapping out these input and corresponding output states with quantum state tomography (QST), using the pulse sequence illustrated in Fig. 3a. The resulting experimental process matrix $\chi_{\rm exp}$ is shown in Fig. 3b together with the ideal matrix $\chi_{\rm id}$ for comparison, which corresponds to a gate fidelity of 0.936 ± 0.013. We also examine the gate performance using interleaved RB, where we insert the CZ gate between random gates from the one- and two-qubit Clifford groups, measuring a fidelity of 0.939 ± 0.011 (see Supplementary Information). The Bell state produced by this gate has a fidelity of 0.949 ± 0.018 and a concurrence of 0.914 ± 0.038.

One important feature of our geometric approach is that it allows direct implementation of the three-qubit CCZ gate, which produces a π-phase shift if and only if all qubits are in $|0\rangle$, without using concatenated two-qubit gates as required in previous experiments[17–21]. The CCZ gate, in combination with single-qubit rotations, is equivalent to the Toffoli gate that inverts the state of the target state conditional on the state of the two control qubits, and which is essential for constructing a universal set of quantum operations[27] and for quantum error correction[17]. We realize the CCZ gate with Q_1, Q_3, and Q_5 by carefully adjusting the qubit level configuration and reconstruct the experimental QPT matrix $\chi_{\rm exp}$ with a fidelity of 0.868 ± 0.004 (Fig. 4). The Ramsey interference patterns of each of the three qubits conditional on the state of the rest two qubits are shown in Supplementary Information, demonstrating that the geometric phase plays a dominant role in the gate implementation.

The dynamical effect, one of the main error sources in both the CZ and CCZ gate implementations, can be suppressed with a new and novel circuit architecture consisting of a coplanar waveguide resonator busing an array of qubits featuring stronger qubit-resonator couplings, larger qubit anharmonicities, and larger differences in qubit anharmonicities, which would enable geometric entangling gates with significantly higher fidelity targeting any two or three qubits in the qubit array. As verified by numerical simulation, for the CCZ gate, if the three qubits have anharmonicities of 0.8, 1.0, and 1.2 GHz, respectively, all coupled to the resonator with $g_{01}/2\pi = 40$ MHz, the gate fidelity can be improved to 0.985 with coherence times around 100 μs.[28] The geometric gates are robust against variations of certain parameters, e.g., a ten percent variation of g_{10} in the above-mentioned calculation only causes the CCZ gate fidelity to fluctuate around one tenth of a percent. We further note that, using qubits with sufficiently large ratios of the anharmonicities to the qubit-resonator couplings, geometric CZ gates can be produced by strongly driving the qubits[30]; within this scenario, the gates can be significantly sped up for reducing the decoherence impact and ultimately for reaching the fidelity threshold for fault-tolerant quantum computing.

Methods

Experimental device. Our circuit QED architecture consists of five frequency-tunable superconducting Xmon qubits[29], all coupled to a bus resonator R with a fixed bare frequency; each qubit can be effectively decoupled from the resonator by tuning it far off-resonant with the resonator. The qubit combinations of Q_3, Q_1-Q_5, and Q_1-Q_3-Q_5 are selected in the one-, two-, and three-qubit experiments, respectively, with Q_2 serving as the microwave bridge through which the resonator can be driven and Q_4 as the meter for measuring the resonator photon number. Each qubit dispersively interacts with its own readout resonator, which couples to a common transmission line for multiplexed readout of all qubits. Single-shot quantum non-demolition measurement is achieved with a home-made impedance-transformed Josephson parametric amplifier whose bandwidth is above 200 MHz at desired frequencies, following the design in Ref.[31]. We can simultaneously probe populations in the ground $|0\rangle$, the first-excited $|1\rangle$, and the second-excited $|2\rangle$ states of all qubits; the $|2\rangle$-state probability is measured in this work for examining the state-leakage error. The device and the measurement setup are sketched in Fig. 1a, with details described in Supplementary Information.

Ramsey-type measurement. The Ramsey interference sequence starts by applying an $X_{\pi/2}$ gate that rotates Q_3 around the x axis on the Bloch sphere by an angle of $\pi/2$, transforming it from the ground state $|0\rangle$ to the superposition state $\left(|0\rangle - i\,|1\rangle\right)/\sqrt{2}$, with the experimental sequence shown in Fig. 1d. Other qubits remain in $|0\rangle$ and are all far-detuned at their individual sweet-point frequencies except for Q_4, which is set 300 MHz below the resonator and will be used for reading out the resonator photon number. Then the external microwave drive Ω is applied, which is blue-detuned from the resonator conditional upon the qubit state $|0\rangle$ by $\delta/2\pi = 4$ MHz. After a duration $T = 250$ ns, the qubit evolves to the state $\left(e^{i\beta}\,|0\rangle - i\,|1\rangle\right)/\sqrt{2}$, with the resonator going back to the ground state. A $\theta_{\pi/2}$ gate is subsequently applied to rotate Q_3 by $\pi/2$ around the axis with a θ-angle to the x axis in the xy plane. Finally the qubit is detected, with the probability of being measured in the state $|1\rangle$ given by $P_1 = \frac{1}{2}\left[1 + \cos(\beta + \theta)\right]$.

[1] Berry, M. V. Quantal phase-factors accompanying adiabatic change. *Proc. R. Soc. Lond. A* **392**, 45-57 (1984).

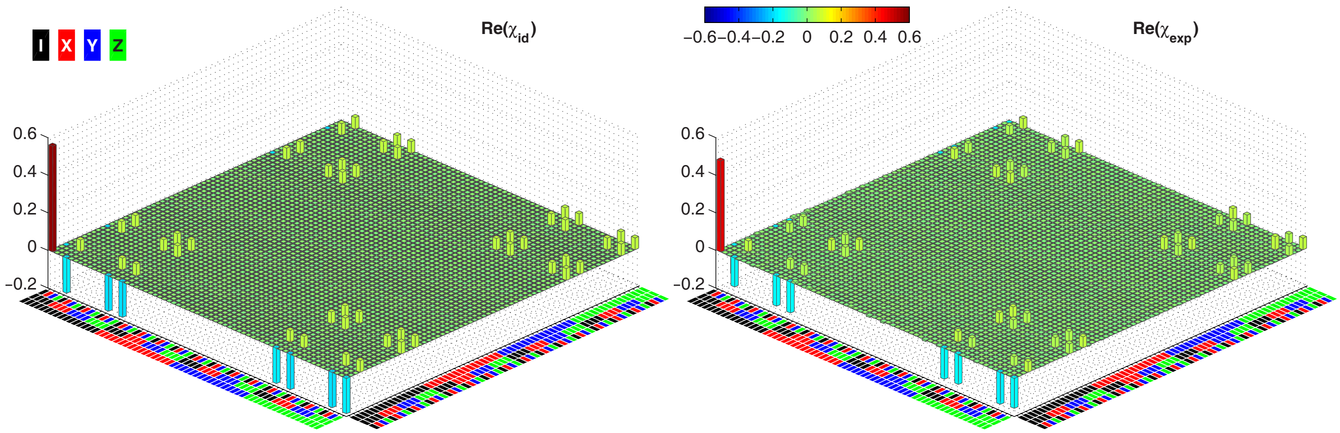

FIG. 4. **QPT of the geometric three-qubit CCZ gate,** obtained with the drive amplitude $\Omega/2\pi = \sqrt{7.5}$ MHz and detuning $\delta/2\pi = 4$ MHz. The color code for Pauli basis {I, X, Y, Z} is shown at the top-left corner. The process matrix is reconstructed by preparing a complete set of 64 input states, and measuring both the input and output density matrices using QST. The ideal ($\chi_{\rm id}$) and experimental ($\chi_{\rm exp}$) quantum process matrices are presented in the left and right panels, respectively. Imaginary components of $\chi_{\rm exp}$ are measured to be no larger than 0.063 in magnitude. The fidelity of $\chi_{\rm exp}$ is 0.868 ± 0.004. The $|2\rangle$-state occupation probability of each qubit resulting from the drive Ω is no higher than 0.025 in a separate measurement, in which the test qubit is initialized in $|1\rangle$ and the other two qubits are in $|0\rangle$.

[2] Aharonov, Y. & Anandan J. Phase-change during a cyclic quantum evolution. *Phys. Rev. Lett.* **58**, 1593-1596 (1987).

[3] Anandan, J. The geometric phase. *Nature* **360**, 307-313 (1992).

[4] Moody, J., Shapere, A. & Wilczek, F. in Geometric phase in physics (eds Shapere, A. & Wilczek, F.) 160-183 (World Scientific, Singapore 1989).

[5] Carollo, A. C. M & Pachos, J. K. Geometric phases and criticality in spin-chain systems. *Phys. Rev. Lett.* **95**, 157203 (2005).

[6] Leibfried, D. et al. Experimental demonstration of a robust, high-fidelity geometric two ion-qubit phase gate. *Nature* **422**, 412-415 (2003).

[7] Jones, J. A., Vedral, V., Ekert, A. & Castagnoli, G. Geometric quantum computation with NMR, *Nature* **403**, 869-871 (2000).

[8] Tycko, R. Adiabatic rotational splittings and Berry's phase in nuclear quadrupole resonance. *Phys. Rev. Lett.* **58**, 2281-2284 (1987).

[9] Suter, D., Mueller, K. T. & Pines, A. Study of the Aharonov-Anandan quantum phase by NMR interferometry. *Phys. Rev. Lett.* **60**, 1218-1220 (1988).

[10] Leek, P. J. *et al.* Observation of Berry's Phase in a Solid State Qubit, *Science* **318**, 1889-1892 (2007).

[11] Filipp, S., Klepp, J., Hasegawa, Y., Plonka-Spehr, C., Schmidt, U., Geltenbort, P. & Rauch, H. Experimental demonstration of the stability of Berry's phase for a spin-1/2 particle, *Phys. Rev. Lett.* **102**, 030404 (2009).

[12] Neely, M. *et al.* Emulation of a Quantum Spin with a Superconducting Phase Qudit. *Science* **325**, 722-725 (2009).

[13] Abdumalikov Jr, A. A., Fink, J. M., Juliusson, K., Pechal, M., Berger, S., Wallraff, A. & Filipp, S. Experimental realization of non-Abelian non-adiabatic geometric gates, *Nature* **496**, 482-485 (2013).

[14] Feng, G., Xu, G. & Long, G. Experimental realization of nonadiabatic holonomic quantum computation, *Phys. Rev. Lett.* **110**, 190501 (2013).

[15] Arroyo-Camejo, S., Lazariev, A., Hell, S. W. & Balasubramanian, G. Room temperature high-fidelity holonomic single-qubit gate on a solid-state spin, *Nature Comm.* **5**, 4870 (2014).

[16] Zu, C., Wang, W.-B., He, L., Zhang, W.-G., Dai, C.-Y., Wang, F. & Duan, L.-M. Experimental realization of universal geometric quantum gates with solid-state spins, *Nature* **514**, 72-75 (2014).

[17] Reed, M. D., DiCarlo, L., Nigg, S. E., Sun, L., Frunzio, L., Girvin, S. M. & Schoelkopf, R. J. Realization of three-qubit quantum error correction with superconducting circuits. *Nature* **482**, 382-385 (2012).

[18] Mariantoni, M. *et al.* Implementing the quantum von Neumann architecture with superconducting circuits. *Science* **334**, 61-65 (2011).

[19] Fedorov, A., Steffen, L., Baur, M. & Wallraff, A. Implementation of a Toffoli gate with superconducting circuits. *Nature* **481**, 170-172 (2012).

[20] Monz, T. *et al.* Realization of the quantum Toffoli gate with trapped ions. *Phys. Rev. Lett.* **102**, 040501 (2009).

[21] Lanyon, B. P. *et al.* Simplifying quantum logic using higher-dimensional Hilbert spaces. *Nature Phys.* **5**, 134-140 (2009).

[22] De Chiara, G. & Palma, G. M. Berry phase for a spin-1/2 particle in a classical fluctuating field, *Phys. Rev. Lett.* **91**, 090404 (2003).

[23] Carollo, A., Fuentes-Guridi, I., Santos, M. F. & Vedral, V. Geometric phase in open systems, *Phys. Rev. Lett.* **90**, 160402 (2003).

[24] Zheng, S. B. Geometric phase for a driven quantum field subject to decoherence. *Phys. Rev. A* **91**, 052117 (2015).

[25] Zhu, S. L. & Wang, Z. D. Unconventional geometric quantum computation. *Phys. Rev. Lett.* **91**, 187902 (2003).

[26] Pechal, M., Berger, S., Abdumalikov, A. A., Fink, J. M., Mlynek, J. A., Steffen, L., Wallraff, A. & Filipp, S. Geometric phase and nonadiabatic effects in an electronic harmonic oscillator. *Phys. Rev. Lett.* **108**, 170401 (2012).

[27] Shi, Y. Both Toffoli and controlled-NOT need little help to do universal quantum computation. *Quantum Inf. Comput.* **3**, 84-92 (2003).

[28] Yan, F. *et al.* The Flux Qubit Revisited to Enhance Coherence and Reproducibility. *Nature Commun.* **7**, 12964 (2016).

[29] Barends, R. *et al.* Coherent Josephson qubit suitable for scalable quantum integrated circuits. *Phys. Rev. Lett.* **111**, 080502 (2013); Kelly, J. *et al.* State preservation by repetitive error detection in a superconducting quantum circuit. *Nature* **519**, 66-69 (2015).

[30] Zheng, S.-B. Quantum-information processing and multiatom-entanglement engineering with a thermal cavity. *Phys. Rev. A* **66**, 060303(R) (2002).

[31] Mutus, J.Y. *et al.* Strong environmental coupling in a Josephson parametric amplifier. *Appl. Phys. Lett.* **104**, 263513 (2014).

Acknowledgments

This work was supported by the Major State Basic Research

Development Program of China (Grants No. 2014CB921201 and No. 2012CB921601), the National Natural Science Foundations of China (Grants No. 11434008, No. 11374054, and No. 11574380), and the Fundamental Research Funds for the Central Universities of China (Grant No. 2016XZZX002-01). Devices were made at the Nanofabrication Facilities at Institute of Physics in Beijing, University of Science and Technology in Hefei, and National Center for Nanoscience and Technology in Beijing.

Author contributions

S.Z. conceived the experiment. C.S., supervised by H.W., carried out the experiment and analyzed the data with supports from S.Z.. H.D. and K.H., supervised by X.Z., fabricated the devices, with designs and supports from W.L., Q.G., and H.W.. S.Z., H.W., and X.Z. cowrote the paper. All authors contributed to the experimental setup and the measurement, and helped to write the paper.